Current Applied Science and Technology Vol. 22 No. 2 (March-April 2022)

Research article

Immobilization of Silver Doped Titanium Dioxide onto Stainless Steel Wire Mesh for Photocatalytic Degradation of Gaseous Formaldehyde under Visible Light Irradiation

Chaval Sriwong[1,2], Akekarat Klypoo[1], Aiyakub Khingram[1], Ratima Natluecha[1] and Suwannee Junyapoon[1]*

[1]*Department of Chemistry, School of Science, King Mongkut's Institute of Technology Ladkrabang, Bangkok, Thailand*
[2]*Center of Excellence in Smart Materials Research and Innovation, King Mongkut's Institute of Technology Ladkrabang, Bangkok, Thailand*

Received: 24 May 2021, Revised: 18 June 2021, Accepted: 12 July 2021

DOI: 10.55003/cast.2022.02.22.001

Keywords

gaseous formaldehyde;

graphene oxide;

photocatalytic degradation;

silver-titanium dioxide;

visible light

Abstract

Titanium dioxide (TiO_2) photocatalysis can degrade air pollutants into nontoxic substances but it can only be excited by UV light. To eliminate this limitation, silver (Ag) and/or graphene oxide (GO) doped TiO_2 are applied to enhance visible light photocatalytic activity. In this study, Ag-TiO_2 (0.5%, 1%, 2% w/w), GO/TiO_2 and GO/Ag-TiO_2 were synthesized and then coated on stainless steel mesh. Crystalline and molecule structures, chemical compositions and optical properties of the prepared photocatalyst samples were characterized with X-ray diffraction spectroscopy, X-ray fluorescence spectroscopy, Raman spectroscopy, UV-visible diffuse reflectance spectroscopy, Fourier-transform infrared spectroscopy, and Scanning electron microscopy equipped with Energy dispersive X-ray spectroscopy techniques. The photocatalytic performances of the various doped catalysts were evaluated according to their abilities to degrade gaseous formaldehyde (HCHO) under visible light. The effect of operational parameters on the photocatalytic degradation of HCHO including layer numbers of photocatalyst, powers of fluorescent lamp and flow rates of HCHO were observed. The results indicated that the presence of Ti, O and Ag elements in Ag-TiO_2 and Ti, O, Ag and C elements in GO/Ag-TiO_2 was confirmed. Proper dispersion of the photocatalyst on the wire mesh was exhibited. Under visible light, the incorporation of Ag and GO in TiO_2 photocatalysts produced higher degradation rates of HCHO than pure TiO_2. The optimum operating conditions of HCHO degradation at initial concentration of 108.7±1.15 ppm over visible light irradiation for 30 min were 5 layers of 0.5% Ag-TiO_2, 72 W fluorescent light and 300 ml/ min of HCHO flow rate. Under these conditions, the removal efficiency of gaseous HCHO was 76.70±0.73%.

*Corresponding author: Tel.: 662-329-8400-11 ext. 290 Fax: 662-329-8428
E-mail: suwannee.ju@kmitl.ac.th

1. Introduction

Titanium dioxide (TiO_2) photocatalysis has been extensively used for the destruction of indoor volatile organic compounds (VOCs) because of its efficient photo-activity, high stability, non-toxicity and low cost [1, 2]. However, there are some limitations due to its low light-harvesting capacity, high energy band gap (about 3.0 eV for rutile and 3.2 eV for anatase) and the high recombination rate of photo-generated electron-hole pairs [3, 4]. In the photocatalytic process, the surface of TiO_2 can be commonly activated by UV radiation, which is harmful to human health causing cataract and skin cancer [5]. In order to overcome these drawbacks, TiO_2 has been modified by doping transition metal particles (i.e. platinum (Pt) [2], zirconium (Zr) [6], nickel (Ni) [7], iron (Fe) [8], silver (Ag) [9, 10], etc.) onto its surface. This leads to a narrow band gap of energy for visible light absorption. In addition, the combination of TiO_2 with graphene oxide (GO) or reduced graphene oxide (rGO) can improve the transfer of photo-generated electrons, and thus reduce the recombination of photo-generated electron-hole pairs (e_{cb}^-/h_{vb}^+) as well as increase the photocatalytic reaction area [11-15].

Formaldehyde (HCHO) is known as one of the highly toxic volatile organic compounds found in indoor air. It is released through off-gassing from building materials and household products, burning of fuels during cooking including tobacco smoking [16]. Many research findings reported that indoor levels of HCHO were significantly higher than the outdoor concentrations [16]. Moreover, they often found levels exceeding the World Health Organization (WHO) guideline of 0.1 mg/m^3 (80 ppb_v) [17]. Inhalation of HCHO can potentially cause coughing, wheezing, nausea, and have other adverse effects on the respiratory tract and so on. Long-term exposure to HCHO is associated with increased risk of certain types of cancer [18]. International Agency for Research on Cancer has classified HCHO as a human carcinogen (Group 1) [19]. Several HCHO removal technologies such as adsorption technology [20], plasma technology [21], biological treatment [22], and advanced oxidation process [2, 6, 11, 13], have recently gained attention. Although adsorption technology is widely used, it has various disadvantages, i.e. limited adsorption capability, short-lifetime, and possibility of pollutant desorption during regeneration [23]. Plasma technology may generate harmful by-products during the degradation process [24] while toxicity of HCHO may inhibit the use of biological treatment methods. Presently, TiO_2-based photocatalysis is regarded as a promising and practical technology to degrade formaldehyde in gas streams. The hydroxyl ($^{\bullet}OH$) and superoxide ($^{\bullet}O_2^-$) radicals are generated on the surface of a photocatalyst. Subsequently, HCHO is completely oxidized to carbon dioxide (CO_2) and water (H_2O) which are non-toxic compounds [10, 25]. However, the use of TiO_2 powder leads to high aggregation tendency and difficulty in separation and recovery. The immobilization of TiO_2 onto different support materials was suggested to overcome these limitations [10, 25-27]. Previous studies reported that immobilization techniques and types of support material used in catalyst preparation significantly influenced the photocatalytic properties of the catalyst [26].

In this study, the photocatalytic degradation of gaseous HCHO using different modified TiO_2 photocatalysts was investigated under visible light irradiation compared with UV-C irradiation and dark conditions. Silver-doped TiO_2 photocatalysts with different metallic contents (0.5% Ag-TiO_2, 1% Ag-TiO_2, 2% Ag-TiO_2), graphene oxide-doped TiO_2 (GO/TiO_2), GO/Ag-doped TiO_2 (GO/Ag-TiO_2) and pure TiO_2 were prepared and coated on stainless steel wire meshes. The physical and chemical properties of the prepared photocatalysts were characterized by X-ray diffraction (XRD), X-ray fluorescence spectrometer (XRF), scanning electron microscope (SEM) equipped with energy dispersive X-ray spectroscopy (EDS), UV-visible diffuse reflectance spectroscopy (UV-vis DRS), Raman spectroscopy and Fourier-transform infrared (FTIR) spectroscopy. Influencing factors on the decomposition of HCHO such as amount of photocatalyst, light intensity,

flow rate of HCHO were examined using the optimum photocatalyst and light source obtained from this study.

2. Materials and Methods

2.1 Chemicals and reagents

Degussa P25 TiO_2 (80:20, Anatase (A)/Rutile (R)) was obtained from Jebsen & Jessen Ingredients (T) Ltd. Graphite powder with an average particle diameter of < 20 μm (99 % purity) was purchased from Aldrich Chemistry (USA). Silver nitrate ($AgNO_3$), formaldehyde (HCHO, 36.5-38%), sulfuric acid (H_2SO_4, 96 wt %), hydrochloric acid (HCl, 37 wt %), sodium nitrate ($NaNO_3$), acetyl acetone ($C_5H_8O_2$, 99.5 wt%), potassium permanganate ($KMnO_4$), and hydrogen peroxide (H_2O_2 30 wt%) were purchased from Carlo Erba Reagents (Italy). Acetic acid (CH_3COOH, 99.85%) was purchased from Duksan Pure Chemical (The Republic of Korea). Ammonium acetate (CH_3COONH_4, 98%) was purchased from Laboratory Reagents & Fine Chemicals (India). All chemical reagents (except ethanol) were analytical grade and used without further purification. Ethanol (C_2H_5OH, 95%) was purchased from the Liquor Distillery Organization, Excise Department, Thailand. Deionized (D.I.) water, produced by a Milli-Q water purification unit (ROM-250-100T, Treat Chemical Co., Ltd), was used for preparation of the solutions.

2.2 Preparation of photocatalyst substrate

50 mesh stainless steel screen, used as a support material, was cut in circle with a diameter of 10 cm. It was initially rubbed with sandpaper. After scrubbing, it was immersed in ethanol for 30 min and then soaked in D.I. water for 10 min to remove oxide and other impurities. The clean screen was dried in a hot air oven at 80°C for 1 h and then kept in a desiccator for further use.

2.3 Preparation of photocatalysts

In this study, titanium dioxide (TiO_2) was used as a photocatalyst. Silver (Ag) and graphene oxide (GO) were applied as co-catalysts on TiO_2 to enhance the photocatalytic activity under visible light. The preparation of the photocatalysts is described as follows:

2.3.1 Preparation of TiO_2 photocatalyst

A TiO_2 photocatalyst was prepared by mixing 4 g of TiO_2 powder with 150 ml of ethanol followed by sonication in an ultrasonic bath for 1 h. The resulting paste was fully spread on the clean disc and then dried in a hot air oven at 80°C for 1 h.

2.3.2 Preparation of Ag-TiO_2 photocatalyst

Silver (Ag), at various contents (0.5%, 1% and 2% w/w), was the metal used for doping TiO_2. The Ag-TiO_2 photocatalysts were prepared by solvothermal process using a modified method of Khalid *et al.* [8, 28]. The $AgNO_3$ solution was dropped into the TiO_2 solution prepared as mentioned in 2.3.1. After stirring for 2 h, the suspension was placed in a 250 ml Teflon-sealed autoclave reactor and then heated in a hot air oven at 150°C for 4 h. The resulting composite was washed with ethanol followed by rinsing with D.I. water twice to remove impurities. Subsequently, it was evaporated to

a volume of 50 ml. The composite paste was fully spread on the clean disc and then dried in a hot air oven at 70°C for 12 h.

2.3.3 Preparation of GO/TiO_2 photocatalyst

Graphene oxide (GO) was synthesized by oxidizing graphite powder with H_2SO_4 and $KMnO_4$ through a modified Hummers method as described in Phrompet *et al.* [29]. A GO/TiO_2 photocatalyst was synthesized with 0.75% of GO to TiO_2 weight ratio, according to the study of Sriwong *et al*. [14]. Initially, the prepared TiO_2 suspension was adjusted to about pH 4 with 1% HCl. Then, 0.75% of GO to TiO_2 weight ratio was gradually added to the TiO_2 suspension while stirring. After the addition, the mixed suspension was further agitated for 1 h at room temperature. The resulting product was washed several times with deionized (D.I.) water and then separated by centrifugation until the supernatant reached pH 7. Afterwards, it was dehydrated to a volume of 50 ml. The resulting paste was fully spread on the clean wire mesh disc and then dried in a hot air oven at 80°C for 8 h.

2.3.4 Preparation of GO/Ag-TiO_2 photocatalyst

In this study, a GO/Ag-TiO_2 photocatalyst was synthesized with 0.09% of Ag to GO/TiO_2 weight ratio (obtained following the result of Khalid and co-workers [30]). Four grams of TiO_2 powder was added to a mixture of D.I. water (70 ml) and ethanol (70 ml) under agitation for 15 min. Later, 400 mg of the synthesized GO was slowly added to the mixture and stirred continuously for an additional 3 h. The resulting mixture was equilibrated by sonication for 1 h. $AgNO_3$ was dissolved in a mixture of acetic acid (5 ml), ethanol (25 ml) and D.I. water (5 ml). The $AgNO_3$ solution was slowly dropped into the synthesized GO/TiO_2 while stirring for another 1 h. Subsequently, the suspension was placed in a 250 ml Teflon-sealed autoclave reactor and heated at 120°C for 3 h in a hot air oven. The GO/Ag-TiO_2 composite was washed with ethanol and then separated by centrifugation followed by rinsing with D.I. water several times. Later, it was dehydrated to a volume of 50 ml. The resulting paste was fully spread on the clean wire mesh disc and then dried in a hot air oven at 70°C for 5 h.

2.4 Characterization

The crystalline structures of TiO_2 (Degussa P25) and Ag-TiO_2 coated on the wire mesh discs were measured using an X-ray diffractometer (XRD-6100, Shimadzu, Japan) with Cu-Kα radiation (40 kV, 30 mA) (λ = 1.5406 Å). Data were taken in the 2θ scan range of 5° to 80° with a step of 0.02° and 0.6 s per step. Diffraction patterns of both anatase and rutile phases of TiO_2 photocatalyst were confirmed with reference to JCPDS database. The element compositions of the prepared photocatalysts were determined with an X-ray fluorescence spectrometer (XRF) (SRS 3400, Bruker AXS, Germany).

The chemical compositions were analyzed by a Raman spectrometry (DXR SmartRaman, Thermo Scientific, USA) using a laser wavelength of 532 nm with power 10 mW. The infrared (IR) spectra of the samples were obtained with a Fourier-transform infrared spectrometer (FTIR) (Nicolet 6700, Thermo Scientific, Germany) using the KBr pellet method. The spectra were recorded in the wavenumber range of 4,000-400 cm^{-1} with a resolution of 4 cm^{-1}. The absorption characteristics were measured on a UV-visible diffuse reflectance spectrometer (UV-vis DRS) (UV-2600, Shimadzu) over the range of 200-800 nm.

A scanning electron microscope (SEM) (Leo 1455 VP, Leo, Germany) equipped with an energy dispersive X-ray spectrometer (EDS) (Xmax50, Oxford, UK) was used to investigate the

surface morphologies of the prepared photocatalyst samples. The energy of the beam was in the range of 5-7 keV. The images were obtained from backscattered electrons.

2.5 Experimental

2.5.1 Photocatalytic reactor

A self-made photocatalytic reactor was composed of a reactor column and a light source housed in a wooden box. The reactor column consisted of 6 clear cylindrical acrylic tubes (internal diameter of 9 cm with the height of 10 cm). Two tubes, used as top and bottom tubes, were closed on top with acrylic lids. An inlet valve was positioned in the bottom tube whereas an outlet valve was placed in the top tube. The reactor column was assembled by placing a stainless steel disc coated with the synthesized photocatalyst between two rubber o-rings followed by two acrylic tubes. These two tubes were connected by tightening with screw knots. The reactor column was tested for gas leak by applying a soap solution to each connection while blowing air through the column. The reactor column was placed in a rectangular wooden box (45 cm length x 50 cm width x 80 cm height) covered with white paper inside to prevent light adsorption. Four sets of 18-W fluorescent lamps and UV-C lamps (Narwar, India) were used as the light source of visible and UV-C radiation, respectively. The lamp was positioned on each side of the box wall.

2.5.2 Experimental procedure

In this study, HCHO was used as an indoor air pollutant to evaluate the photocatalytic activity of the synthesized photocatalysts. The amount of HCHO was determined by the acetylacetone spectrophotometric method [31]. The measurement procedure of initial concentration of gaseous HCHO is illustrated in Figure 1(a). A batch experiment was conducted as follows: Firstly, 200 ml of 1% (v/v) HCHO solution was placed in a 250 ml Erlenmeyer flask (flask no. 1). Secondly, it was heated with a hot plate at a temperature of 70°C while air was blown through the solution at flow rate of 500 ml/min for 30 min. The gaseous HCHO was passed through an empty flask (flask no. 2) to remove water vapor and then collected in a three-step sequential absorbing solution (flasks no. 3, 4, 5) containing 200 ml of 1;1:1 mixture (by volume) of ammonium acetate (1.80 mol/l), acetic acid (0.05 mol/l) and acetylacetone (0.02 mol/l). Thirdly, the air flow was passed through the photocatalytic reactor containing three layers of stainless steel disc coated with the synthesized photocatalyst. Fourthly, air flow rate was measured by a gas flow calibrator (Defender 520-H, Bios International Corp., USA) after passing through activated carbon (flasks no. 6, 7) to remove impurities. Finally, the amount of HCHO in the absorbing solution was immediately measured using a UV-vis spectrophotometer (UH 5300, Hitachi, Japan) with a wavelength of 411 nm. The initial concentration of gaseous HCHO was calculated from the sum of three absorbance values to obtain one value. The experiment of HCHO degradation was conducted with a similar procedure to the one mentioned above, but the gaseous HCHO was passed through the photocatalytic reactor in the presence of visible light obtained from 72 W-fluorescent lamps before trapping in the absorbing solutions as illustrated in Figure 1(b). Different types of synthesized photocatalysts (e.g., pure TiO_2, 0.5% Ag-TiO_2, 1% Ag-TiO_2, 2% Ag-TiO_2, GO/TiO_2, GO/Ag-TiO_2) were studied for their ability to photodegrade HCHO. The same experimental procedures were performed using 72 W UV-C lamps. The adsorption capacity of the synthesized photocatalysts was also investigated under dark conditions.

A series of experiments were also conducted to evaluate the factors influencing the photocatalytic degradation of HCHO. The effect of photocatalyst dosage was examined by varying layers of the photocatalyst disc (1, 3, 5 layers) under the following conditions: electric power 72

W-fluorescent lamp, HCHO flow rate 500 ml/min, irradiation time 30 min. The optimum dosage of photocatalyst was selected and then used for the subsequent set of experiments. Later, an experiment was carried out to investigate the effect of light intensity by varying electric powers of fluorescent lamp (18, 36, 72 W). The optimum photocatalyst dosage and light intensity from the study were used to evaluate the effect of reaction time and HCHO concentration by varying flow rates of HCHO (200, 300, 500 ml/min). All sample measurements were performed in triplicate. The experiment was conducted in the fume hood under ambient conditions. The reuse of photocatalyst was not evaluated in this study.

% Removal of HCHO was calculated by equation 1:

$$\%\ Removal\ =\ \left(\frac{C_0-C}{C_0}\right)\ x\ 100 \qquad (1)$$

Where C_0 is the initial concentration of HCHO (ppm) and C is the concentration of the remaining HCHO (ppm).

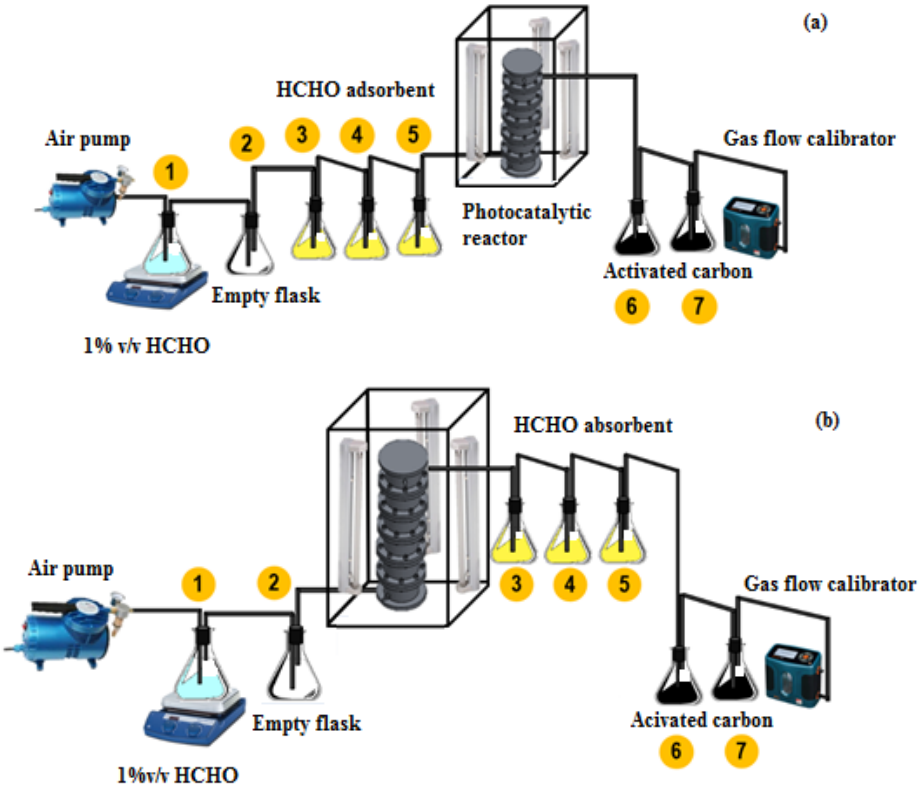

Figure 1. The experimental setup for photocatalytic degradation of HCHO
(a) measurement of initial concentration of HCHO, (b) measurement of the remaining HCHO concentration after treatment; 1) 1% v/v HCHO, 2) Empty flask, 3-5) HCHO absorbents, and 6-7) Activated carbons

2.5.3 Statistical analysis

The data were statistically analyzed by One-way and Two-way analysis of variance (ANOVA), with Fisher's Least Significant Difference (LSD) post hoc test at confidence level of 95%.

3. Results and Discussion

3.1 Characteristics of photocatalysts

XRD patterns confirmed the presence of both anatase (A) and rutile (R) phases of TiO_2 and 0.5% Ag-TiO_2 photocatalysts coated on the wire supports as shown in Figure 2. According to JCPDS, the strong diffraction peaks at 25.40° (101) and 48.08° (200) indicate anatase phase whereas the 2θ peak at 27.36° (110) confirms rutile structure [14, 30]. These confirmed the existence of both anatase and rutile phases of the commercial TiO_2 (Degussa P25). It was noted that all the intensity diffraction peaks of Ag-TiO_2 were lower than those of the pure TiO_2 photocatalyst. This result may be due to the corporation of Ag particles into the TiO_2 surface to form the composite materials. This result agreed with the EDS mapping images in Figures 3(c) and 4(b). Ag particles had been well-incorporated and covered onto the TiO_2 particles. In addition, the diffraction peak at 2θ around 45° likely indicated the presence of Fe metal in the wire dish substrate [32].

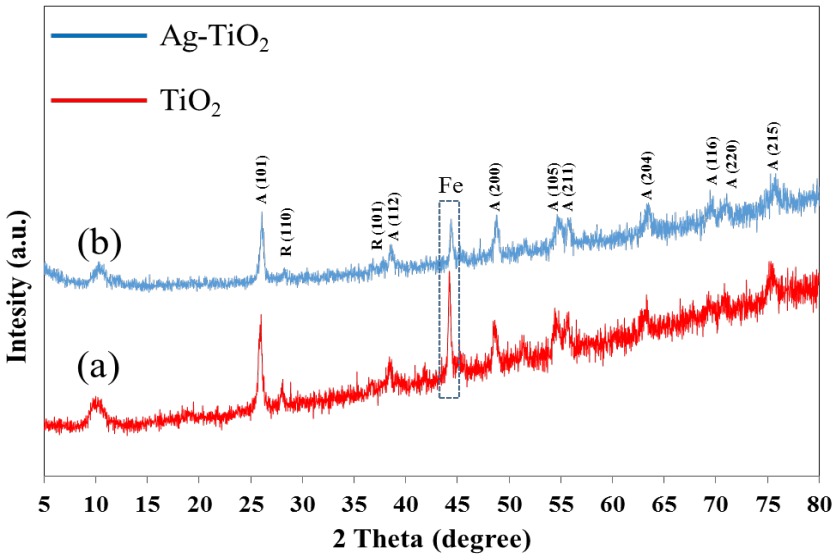

Figure 2. XRD patterns of (a) TiO_2, and (b) 0.5% Ag-TiO_2 photocatalyst coated on wire mesh discs

The element compositions of the synthesized photocatalysts were determined using an energy dispersive X-ray spectrometer, and the results are shown in Figure 3. Si, Mn, Ni, Cr, P, and O atoms were found in the pristine wire disc (Figure 3a). This finding is in alignment with the result of XRF presented in Table 1. Ti and O atoms confirmed the presence of TiO_2 (Figure 3b) whereas Ti, O and Ag atoms confirmed the existence of Ag-TiO_2 (Figure 3c). Ti, O and C were detected in the GO/TiO_2 photocatalyst (Figure 3d). The appearance of Ti, O, C and Ag atoms was confirmed

the presence of GO/Ag-TiO_2 (Figures 3(e). The EDS spectra in Figure 4(c) clearly confirmed the existence of the elements Ti, O and Ag in the 0.5% Ag-TiO_2 photocatalyst.

Table 1 illustrates the element compositions of the synthesized photocatalysts determined by XRF. Titanium (Ti) and oxygen (O) elements were found in all synthesized photocatalysts, confirming the existence of TiO_2. The modified TiO_2 contained lower amounts of Ti compared to pure TiO_2. This may be due to the deposition of co-doping materials on the TiO_2 surface. Silver (Ag) was not detected in Ag-TiO_2 and GO/Ag-TiO_2 whereas carbon (C) was not identified in the GO-TiO_2 and GO/Ag-TiO_2 photocatalysts. This was probably because a very small amount of $AgNO_3$ precursor and GO was doped onto TiO_2 during the preparation. The absence of GO and Ag peaks in the photocatalyst composite was also reported in previous work [30]. However, both C atom and Ag atom were identified by EDS technique, as shown in Figures 3 and 4. Additionally, a major element, iron (Fe), and minor elements such as chromium (Cr), nickel (Ni), manganese (Mn), silicon (Si), copper (Cu) and aluminum (Al) were observed in the synthesized photocatalysts. This may be due to the compositions of stainless steel wire mesh used as a substrate.

Table 1. Element components of the synthesized photocatalysts determined by XRF

Type of photocatalyst	Element components (%)									
	Ti	O	Cr	Mn	Fe	Co	Ni	Cu	Al	Si
Pure TiO_2	12.3	32.3	14.5	0.804	35.2	0.139	3.50	0.193	0.586	0.385
2% Ag-TiO_2	11	32.3	15.1	0.990	32.1	0.151	3.55	0.149	0.713	0.650
GO-TiO_2	9.48	31.8	15.3	1.08	37.2	0.153	3.79	0.198	n.d.	0.596
GO/Ag-TiO_2	2.89	30.9	15.6	1.25	43.4	0.196	4.96	0.198	n.d.	0.917

Figure 5(a) shows the Raman spectra of all synthesized photocatalysts. It can be observed that a strong intensity peak located at 148.14 cm^{-1} (E_g) and a low intensity peak placed at 397.88 cm^{-1} (B_{1g}) related to bridge oscillation of O−Ti−O bending. Meanwhile, peaks at 516.96 cm^{-1} (A_{1g}) and 639.42 cm^{-1} (E_g) indicated Ti−O strain oscillation. This result confirmed the presence of Raman active modes of TiO_2 material which were similar to those reported by Castrejón-Sánchez and Camacho-López [33]. Moreover, two typical peaks of G-band around at 1,594 cm^{-1} and D-band at 1,368 cm^{-1} were detected in GO-TiO_2 and GO/Ag-TiO_2. The G-band indicated graphitic sp^2 carbon structure whereas the D-band showed disordered sp^3 carbon atoms, all of which suggested the presence of graphitic materials [12]. It can be noted that the peaks of G and D bands in GO/Ag-TiO_2 were slightly shifted from those of GO-TiO_2. This was probably due to the effect of Ag addition [34]. Besides, the broad peaks of TiO_2 active modes in GO/Ag-TiO_2 were also observed. This may be because of the interaction of Ag, GO and TiO_2 particles. The FTIR spectra of the photocatalysts in the range of 4,000-400 cm^{-1} are shown in Figure 5(b). The appearance of the broad bands around 800-500 cm^{-1} in all photocatalysts corresponded to the stretching vibrations of Ti-O-Ti bond. These results confirmed the formation of metal oxygen bonding [35]. Small peaks at around 1,600 cm^{-1} observed in GO/Ag-TiO_2, GO-TiO_2 and Ag doped TiO_2 indicated the O-H bending vibration of absorbed water molecules. Meanwhile, the O-H stretching vibration at wave number around 3,400 cm^{-1} of water molecules was also observed. During photocatalysis, the hydroxyl groups (-OH) of the water molecules can act as scavengers of photogenerated electrons and holes, leading to the formation of OH radicals (•OH), a process that results in high photocatalytic activity of the photocatalyst [35, 36]. The optical absorption properties of the synthesized photocatalysts investigated by UV-vis DRS absorption at wavelengths of 200-800 nm are shown in Figure 5(c). It was seen that the UV light absorption (<400 nm) of GO-TiO_2 and pure TiO_2 was obviously stronger than that of Ag-doped TiO_2 and GO/Ag-TiO_2. On the contrary, the visible light absorption of pure

TiO_2 (400-700 nm) was weaker than that of the modified TiO_2 photocatalysts. The spectrum of GO/TiO_2 displays higher absorption intensity in the range of both UV light and visible light than that of pure TiO_2 due to the formation of Ti-O-C bond through an interaction between the unpaired π-electrons of GO and O atoms of TiO_2 [37, 38]. GO has relatively narrow band gaps; thus, it enhances the long wavelength response [38]. The spectra of Ag-doped TiO_2 and GO/Ag-TiO_2 exhibit lower absorption intensities of UV irradiation but they indicate higher absorption intensities of visible light than those of pure TiO_2. The absorption band edges of pure TiO_2, Ag-TiO_2, GO-TiO_2, and GO/Ag-TiO_2 photocatalysts appeared in the range of 392-433 nm, and corresponded to

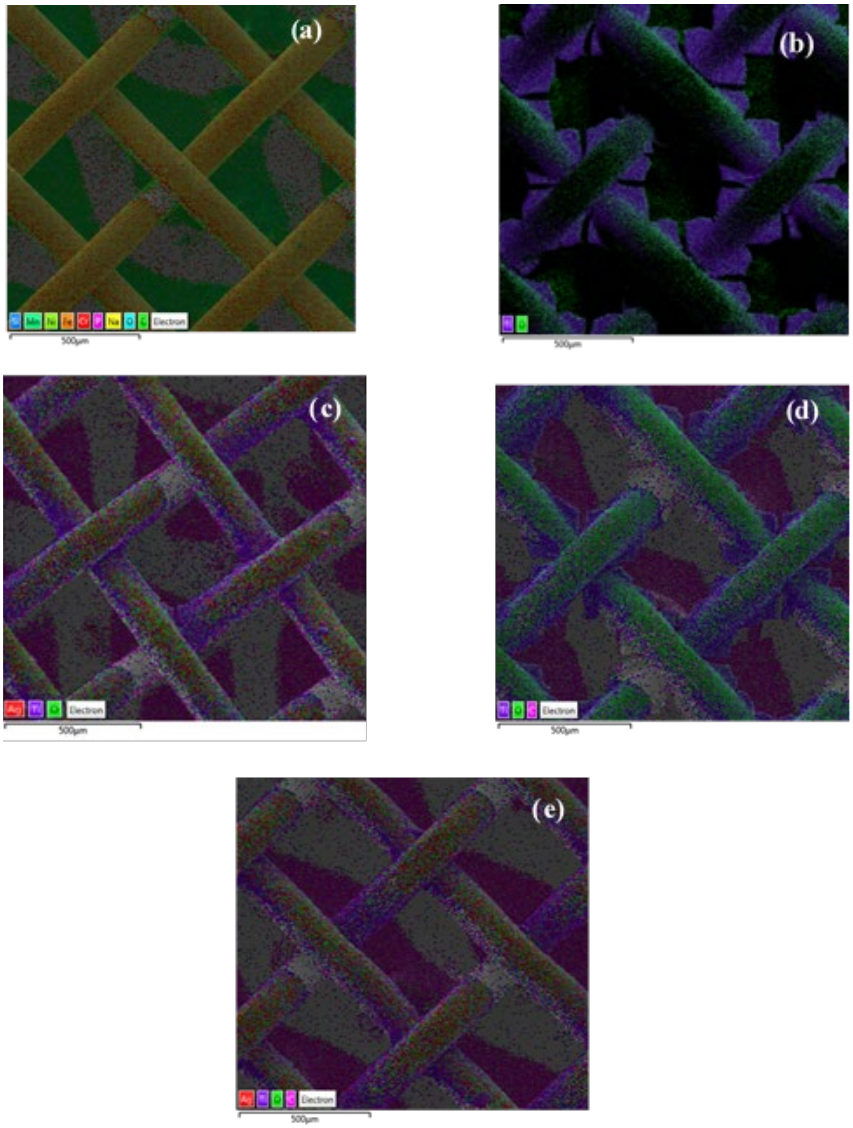

Figure 3. Surface morphologies of the synthesized photocatalysts coated on wire discs measured by EDS (a) wire disc (without coating), (b) TiO_2, (c) 0.5% Ag-TiO_2, (d) GO/TiO_2, and (e) GO/Ag-TiO_2

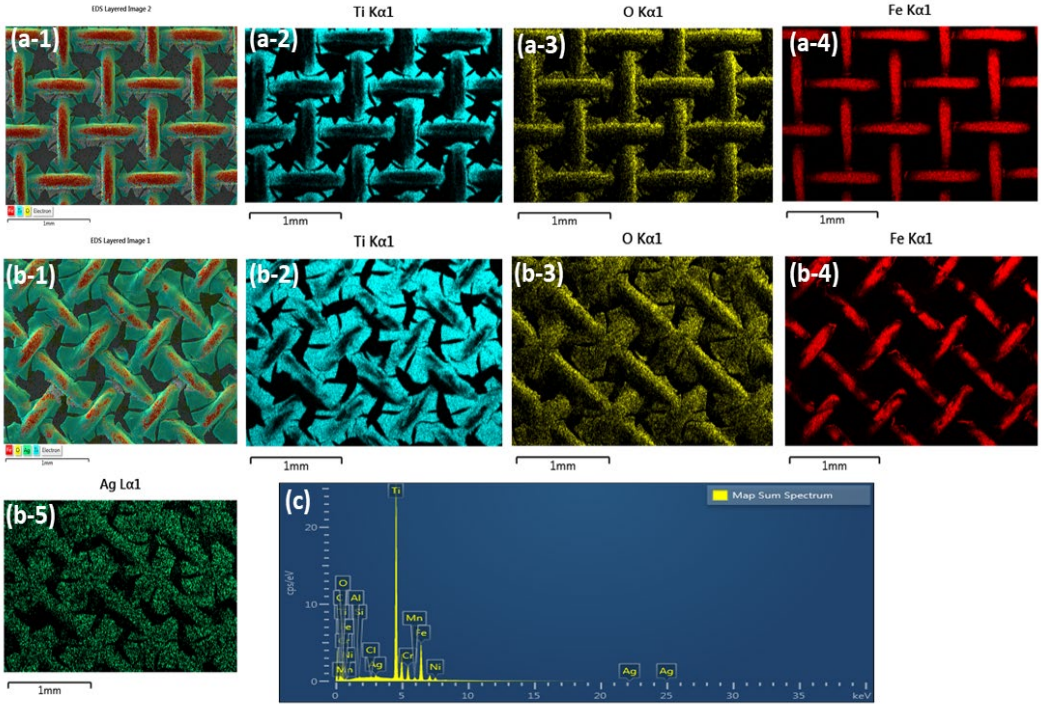

Figure 4. Surface morphologies of the synthesized photocatalysts coated on wire discs measured by EDS (a) TiO_2, (b) 0.5% Ag-TiO_2, and (c) EDS spectra of 0.5% Ag-TiO_2

the band gap energies of 3.16, 3.08, 2.99, and 2.86 eV, respectively. When compared with the pure TiO_2, the absorption band edges of Ag-doped TiO_2 and GO/Ag-TiO_2 shifted to longer wavelengths. This suggested that these photocatalysts were more effective in absorbing the visible light region owing to their smaller band gaps. Meanwhile, the increased absorption in visible light region likely originated from the strong interaction between TiO_2 and GO particles. The incorporation of Ag or GO in TiO_2 nanoparticles resulted in a reduction of band gap energy, enhancing the ability of these photocatalysts to degrade gaseous HCHO with visible light irradiation.

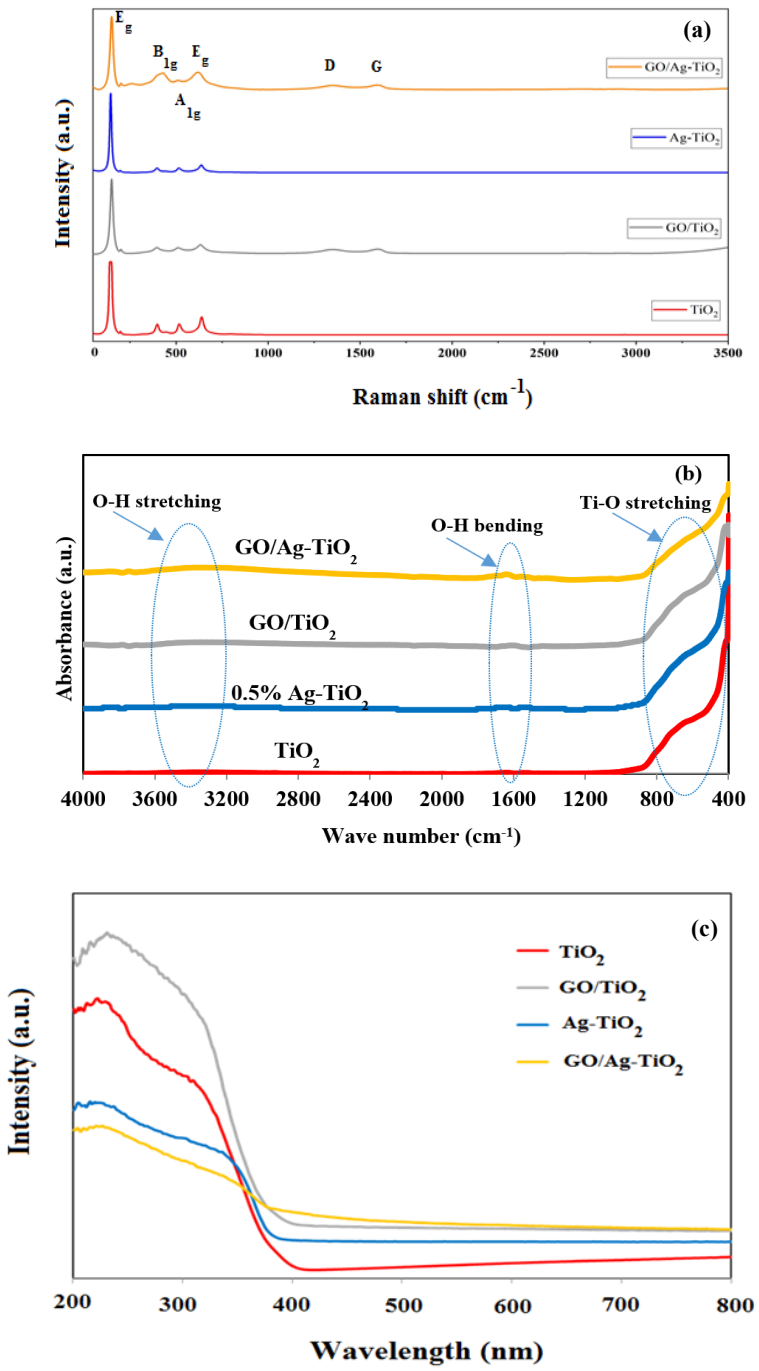

Figure 5. Raman spectra (a), FTIR spectra (b), and UV-vis DRS spectra (c) of the synthesized photocatalysts.

3.2 Photocatalytic degradation

Figure 6 shows the effect of different photocatalyst types (pure TiO_2, 0.5% Ag-TiO_2, 1% Ag-TiO_2, 2% Ag-TiO_2, GO/TiO_2, Ag-TiO_2/GO) and light sources (UV-C, visible light, without light) on the photodegradation of gaseous HCHO. The analysis of data using Two-way ANOVA with Fisher's Least Significant Difference (LSD) post hoc test reveals that variation of both photocatalyst type and light source significantly affected the photocatalytic degradation of gaseous HCHO ($p<0.05$).

Under dark condition, the amounts of gaseous HCHO adsorbed on pure TiO_2, 0.5% Ag-TiO_2, 1% Ag-TiO_2, 2% Ag-TiO_2, GO/TiO_2, GO/Ag-TiO_2 were 35.56±0.89%, 34.72±1.03%, 34.46±1.87%, 33.96±2.10%, 30.53±0.88% and 28.53±0.60%, respectively. There was no significant difference in the adsorption capacity between pure TiO_2 and Ag-doped TiO_2 with different metallic content (0.5%, 1% and 2% w/w) at 95% confidence level. The amount of gaseous HCHO adsorbed on GO/TiO_2 and GO/Ag-TiO_2 was slightly less than that of pure TiO_2 and Ag-doped TiO_2. It was clearly found that gaseous HCHO was adsorbed on the surface of TiO_2 photocatalyst. Doping with Ag and GO may have slightly restricted the surface area of TiO_2.

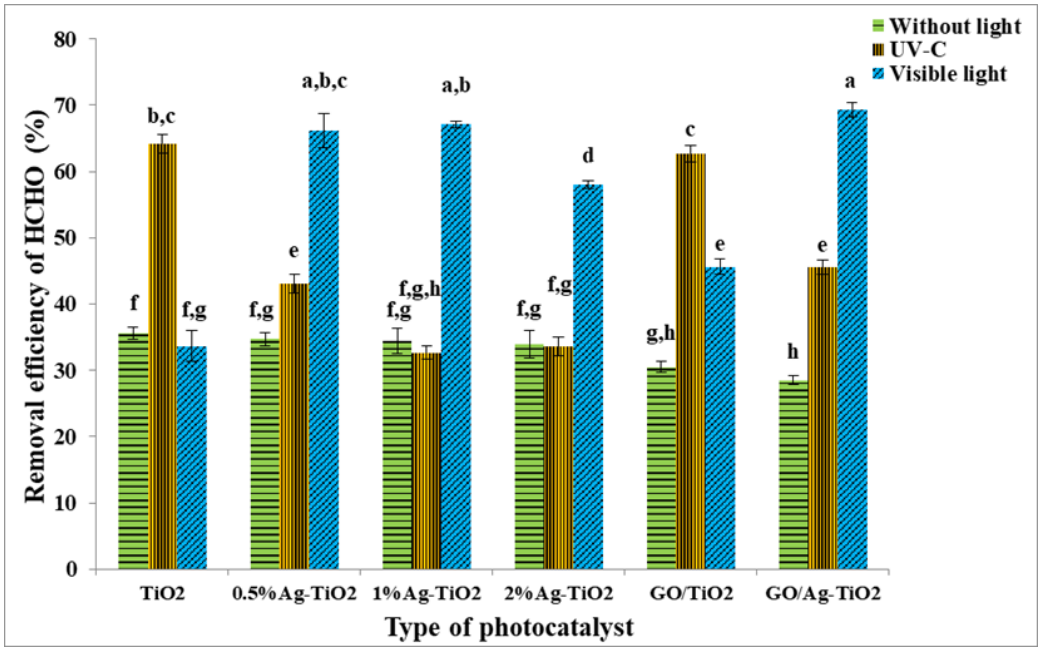

Figure 6. Comparison on removal efficiencies of HCHO by different types of photocatalysts with UV-C irradiation, visible light and without light

Under UV-C irradiation, the removal efficiencies of gaseous HCHO by pure TiO_2, 0.5% Ag-TiO_2, 1% Ag-TiO_2, 2% Ag-TiO_2, GO/TiO_2, GO/Ag-TiO_2 were 64.20±1.38%, 43.01±1.41%, 32.68±0.95%, 33.62±1.39%, 62.65±1.21% and 45.50±1.10%, respectively. The photocatalytic activity of pure TiO_2 was similar to that of GO/TiO_2 ($p<0.05$). The HCHO removal efficiencies of both pure TiO_2 and GO/TiO_2 photocatalysts were about 20% greater than those of GO/Ag-TiO_2 and 0.5% Ag-TiO_2. Pure TiO_2 and GO/TiO_2 showed the highest photocatalytic degradation of HCHO due to their stronger UV absorption (see in Figure 5c) which is corresponding to the work of Yoon and co-workers [39]. When TiO_2 is excited with ultraviolet (UV) irradiation, the valence electrons can transit to the conduction band across the band gap producing electrons (e_{cb}^-) in the conduction

band and positive holes (h_{vb}^{+}) in the valence band, as shown in reaction (1). A photo-induced electron (e_{cb}^{-}) is trapped by oxygen (O_2) forming a superoxide radical anion ($^{\bullet}O_2^{-}$) as illustrated in reaction (2) while the photo-induced positive hole (h_{vb}^{+}) is captured by a water (H_2O) molecule generating hydroxyl radical ($^{\bullet}OH$) as presented in reaction (3) [40]. Then, HCHO is oxidized by $^{\bullet}OH$ and/or $^{\bullet}O_2^{-}$ resulting in the formation of formic acid (HCOOH) as an intermediate (reactions (4)-(6)). Subsequently, the HCOOH is oxidized to carbon dioxide (CO_2) and water (H_2O), which are non-toxic substances as illustrated in reactions (7)-(8) [10, 27].

$$TiO_2 + h\nu \rightarrow h_{vb}^{+} + e_{cb}^{-} \quad (1)$$

$$O_2 + e_{cb}^{-} \rightarrow {}^{\bullet}O_2^{-} \quad (2)$$

$$H_2O + h_{vb}^{+} \rightarrow {}^{\bullet}OH + H^{+} \quad (3)$$

$$HCHO + {}^{\bullet}OH \rightarrow HCO^{\bullet} + H_2O \quad (4)$$

$$HCO^{\bullet} + {}^{\bullet}OH \rightarrow HCOOH \quad (5)$$

$$HCO^{\bullet} + {}^{\bullet}O_2^{-} \rightarrow HCO_3^{-} \xrightarrow{+H^{+}} H_2CO_3 \xrightarrow{+HCOO^{-}} HCOOH + HCO_3^{-} \quad (6)$$

$$HCOOH \xrightarrow{-H^{+}} HCOO^{-} \xrightarrow{h_{vb}^{+}} H^{+} + {}^{\bullet}CO_2^{-} \quad (7)$$

$${}^{\bullet}CO_2^{-} + H^{+} \xrightarrow{[O][OH][h_{vb}^{+}]} CO_2 + H_2O \quad (8)$$

There was no significant difference in the removal of HCHO with 1% Ag-TiO_2 and 2% Ag-TiO_2 during photocatalysis under UV-C radiation and adsorption under dark conditions. This may be because the higher content of Ag may cover the surface of TiO_2, resulting in a reduction of TiO_2 photocatalytic activity.

Under visible light, the removal efficiencies of gaseous HCHO by pure TiO_2, 0.5% Ag-TiO_2, 1% Ag-TiO_2, 2% Ag-TiO_2, GO/TiO_2, Ag-TiO_2/GO were 33.63±2.32%, 66.23±2.58%, 67.08±0.49%, 58.00±0.53%, 45.64±1.17% and 69.26±1.06%, respectively. The removal ability was in the following order: GO/Ag-TiO_2 ≈ 0.5% Ag-TiO_2 ≈ 1% Ag-TiO_2 > 2% Ag-TiO_2 > GO/TiO_2 > pure TiO_2. These results are likely to comply with the absorbance intensity of the photocatalysts in visible region except in the case of GO/TiO_2 as shown in Figure 5c. GO/Ag-TiO_2 and Ag-doped TiO_2 with different metallic content (0.5% and 1% w/w) exhibited greater photocatalytic activity under visible light compared to UV-C irradiation. When doping Ag on TiO_2, the absorption edge might shift from lower wavelength (UV irradiation) to higher wavelength (visible light) owing to the decreased band gap energy of TiO_2 [9, 10]. Thus, the ability of these photocatalysts to degrade gaseous HCHO under visible light irradiation can be enhanced. Moreover, the introduction of Ag and GO onto the interface of TiO_2 particles clearly increased photocatalytic activity under visible light. This can be explained that doping with GO could enhance the separation of photogenerated electron-holes pairs of TiO_2 particles due to its excellent electron acceptor and mobility, leading to the improved photocatalytic efficiency. Doping with Ag can reduce band gap energy of TiO_2 and then shift the absorption band to the visible region [7, 35]. In addition, Ag can produce oxygen anion radicals (O_2^{-}) and reactive center (Ti^{3+}) to prevent recombination of electrons-holes pairs, as shown in reactions (9)-(11) [41].

$$e^- + Ag \rightarrow Ag^- \quad (9)$$

$$Ag^- + O_2 \rightarrow Ag + O_2^- \quad (10)$$

$$Ag^- + Ti^{4+} \rightarrow Ag + Ti^{3+} \quad (11)$$

A possibility of photocatalytic mechanism pathway of Ag-TiO_2 photocatalyst for HCHO degradation under visible irradiation is shown in Figure 7. According to the small band gap of Ag-TiO_2 photocatalyst, electron-hole pairs are generated when visible light hits the Ag-TiO_2 surface. A positive hole (h^+) in the valence band (VB) can react with H_2O or OH^-, transforming them to $^{\bullet}OH$ whereas a negative electron (e^-) in the conduction band (CB) can directly react with oxygen or Ag particles producing oxygen anion radical (O_2^-) and Ag^- ion, respectively. This result prevents the recombination of electrons-holes pairs [40]. After the $^{\bullet}OH$ radical is produced, it can directly attract HCHO molecule forming both H_2O and CO_2 molecules as the final products. However, the photocatalytic activity of 2% Ag-TiO_2 photocatalyst significantly decreased under visible light. This can be explained that the high recombination of photoexcited electrons-hole pairs may occur when excess Ag was doped on TiO_2, resulting in reduced photocatalytic activity [30]. In this study, the photocatalytic capabilities of GO/Ag-TiO_2, 0.5% Ag-TiO_2 and 1% Ag-TiO_2 were not significantly different ($p<0.05$). Therefore, 0.5% Ag-TiO_2 was used as the effective photocatalyst under visible light in the next study. The results showed that these photocatalysts exhibited both photocatalytic activity and adsorption properties, a result which was consistent with the findings of Noguchi and co-workers [42].

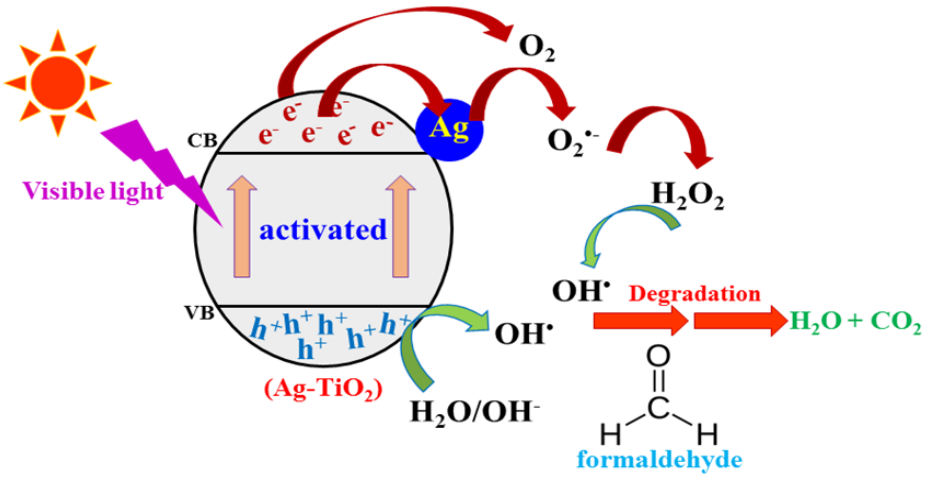

Figure 7. A schematic diagram showing a possible photocatalytic mechanism for Ag-TiO_2 photocatalyst of HCHO degradation under visible light irradiation

Figure 8(a) shows that the removal efficiency of HCHO at 1, 3 and 5 layers of the discs coated with 0.5% Ag-TiO_2 under visible light were 25.62±0.75%, 65.20±2.66% and 75.74±1.09%, respectively. The photocatalytic degradation efficiency of 0.5% Ag-TiO_2 tended to increase with increasing layers of the photocatalyst discs due to the increased number of photocatalytic active

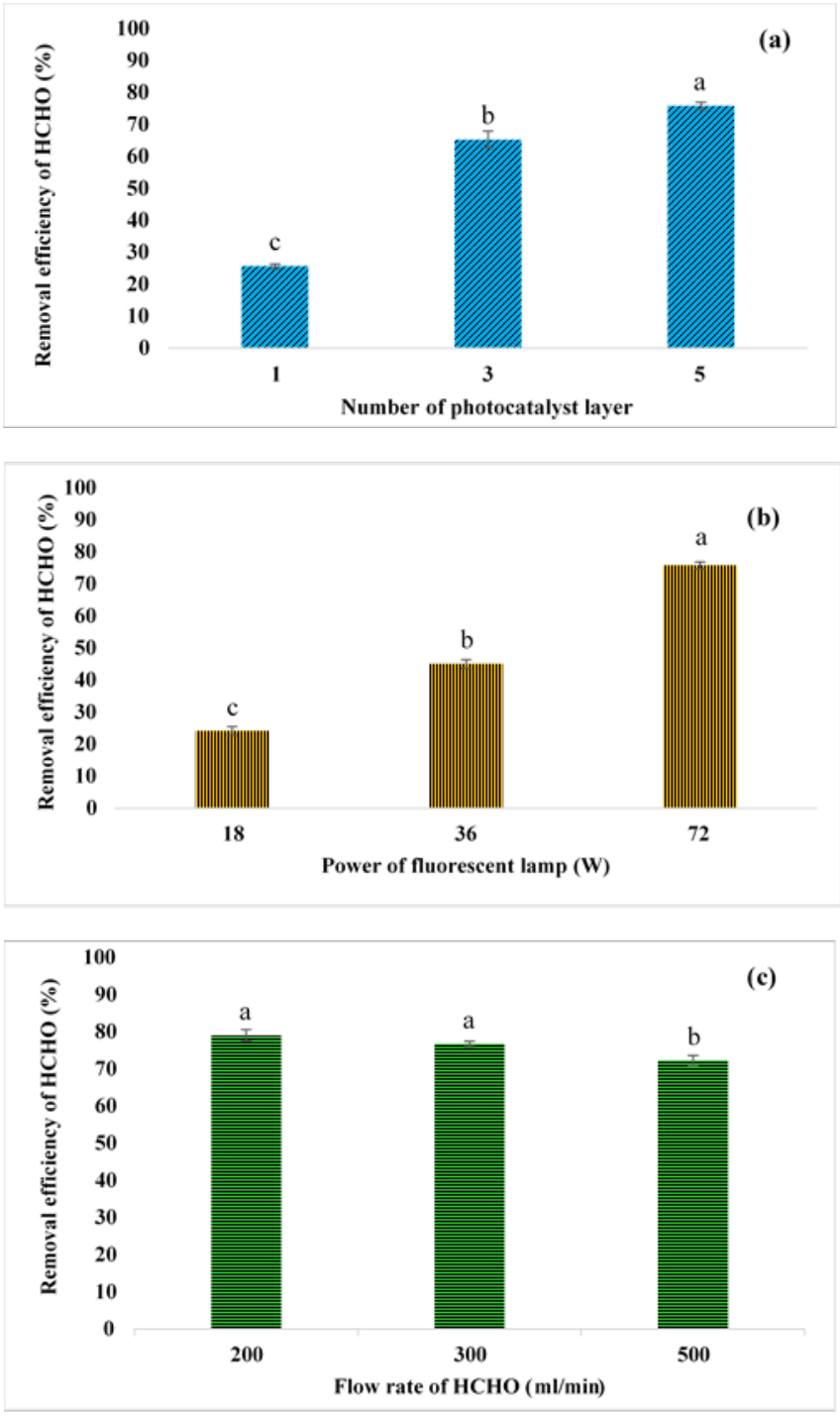

Figure 8. The factors influencing the removal of HCHO: (a) effect of layer number of photocatalyst disc, (b) effect of light intensity, and (c) effect of flow rate of HCHO by 0.5% Ag-TiO_2 under visible light irradiation

sites. The removal efficiencies of HCHO under energy power of 18, 36 and 72 W were 24. 03±1. 31%, 45. 03±1. 38% and 75. 74±1. 09%, respectively, as shown in Figure 8(b). The photocatalytic degradation efficiency of 0.5% Ag-TiO_2 tended to increase with increasing intensity of light. This was probably because the increased fluorescent power resulted in a stronger energy that could separate the electron-hole pairs. The removal efficiency of HCHO at flow rates of 200, 300 and 500 ml/min was 78.99±1.52%, 76.70±0.73% and 72.22±1.41%, respectively (Figure 8(c)). The removal efficiency of HCHO tended to decrease with increasing flow rate of HCHO. This was probably due to the decreased irradiation time as well as the increased loading dose of the pollutant. The evaluation of data using one-way ANOVA with Fisher's Least Significant Difference (LSD) post hoc test shows that the number of layers of the discs coated with 0.5% Ag-TiO_2, energy power, and flow rate of HCHO affected the removal efficiency of HCHO. In this study, there was no significant difference between the removal efficiencies of HCHO at 200 ml/min and 300 ml/min. Thus, the flow rate of HCHO at 300 ml/min was used as the optimum condition because the loading amount of HCHO at flow rate of 300 ml/min was much higher than that of 200 ml/min.

4. Conclusions

Ag doped TiO_2 with different metallic content (0.5%, 1% and 2% w/w), GO/TiO_2 and GO/Ag-TiO_2 photocatalysts coated on wire dish stainless steel substrates were able to improve the photocatalytic activity in the visible light region. These photocatalysts could be applied onto the stainless steel substrate without adding any binder. In this study, 0.5% Ag-TiO_2 was successfully used as an effective photocatalyst with high activity on the degradation of HCHO under visible light. The optimum operating conditions for HCHO photodegradation at initial concentration of 108.7±1.15 ppm over visible light irradiation for 30 min were 5 layers of the stainless steel disc coated with 0.5% Ag-TiO_2, fluorescent power 72 W, and flow rate of HCHO 300 ml/ min. Under these conditions, the removal efficiency of gaseous formaldehyde was 76.70±0.73%.

5. Acknowledgements

This work was supported by School of Science, King Mongkut's Institute of Technology Ladkrabang (KMITL) under Research Grant No. 2562-01-05-22 The authors are grateful to Jebsen & Jessen Ingredients (T) Ltd. for the supply of Degussa P25 TiO_2. The authors are also thankful to staff members of Department of Chemistry, School of Science and College of Nanotechnology, KMITL for their assistance.

References

[1] Shah, K.W. and Li, W., 2019. A review on catalytic nanomaterials for volatile organic compounds VOC removal and their applications for healthy buildings. *Nanomaterials*, 9(6), 910, https://doi.org/10.3390/nano9060910.

[2] Su, Y., Ji, K., Xun, J., Zhang, K., Liu, P. and Zhao, L., 2021. Catalytic oxidation of low concentration formaldehyde over Pt/TiO_2 catalyst. *Chinese Journal of Chemical Engineering*, 29, 190-195.

[3] Schneider, J., Matsuoka, M., Takeuchi, M., Zhang, J., Horiuchi, Y., Anpo, M. and Bahnemann, D.W., 2014. Understanding TiO_2 photocatalysis: mechanisms and materials. *Chemical Reviews*, 114, 9919-9986.

[4] Xu, T., Hong, Z. and Zhang, P., 2018. Performance of an innovative VUV-PCO purifier with nanoporous TiO_2 film for simultaneous elimination of VOCs and by-product ozone in indoor air. *Building and Environment*, 142, 379-387.

[5] Sharma, S., Lang, C., Khadka, J. and Inacio, M.C., 2020. Association of age-related cataract with skin cancer in an Australian population. *Investigative Ophthalmology Visual Science*, 61(5), 48, https://doi.org/10.1167/iovs.61.5.48.

[6] Huang, C., Ding, Y., Chen, Y., Li, P., Zhu, S. and Shen, S., 2017. Highly efficient Zr doped-TiO_2/glass fiber photocatalyst and its performance in formaldehyde removal under visible light. *Journal of Environmental Sciences*, 60, 61-69.

[7] Suligoj, A., Arcon, I., Mazaj, M., Drazic, G., Arcon, D., Cool, P., Stangar, U.L. and Tusar, N.N., 2018. Surface modified titanium dioxide using transition metals: nickel as a winning transition metal for solar light photocatalysis. *Journal of Materials Chemistry A*, 6, 9882-9892.

[8] Khalid, N.R., Hong, Z., Ahmed, E., Zhang, Y., Chan, H. and Ahmad, M., 2012. Synergistic effects of Fe and graphene on photocatalytic activity enhancement of TiO_2 under visible light irradiation. *Applied Surface Science*, 58, 5827-5834.

[9] Fang, R.M., He, M., Huang, H.B., Feng, Q.Y., Ji, J., Zhan, Y.J., Leung, D.Y.C. and Zhao, W., 2018. Effect of redox state of Ag on indoor formaldehyde degradation over Ag/TiO_2 catalyst at room temperature. *Chemosphere*, 213, 235-243.

[10] Gao, L.K., Gan, W.T., Xiao, S.L., Zhan, X.X. and Li, J., 2015. Enhancement of photo-catalytic degradation of formaldehyde through loading anatase TiO_2 and silver nanoparticle films on wood substrates. *RSC Advances*, 5, 52985-52992.

[11] Low, W. and Boonamnuayvitaya, V., 2013. Enhancing the photocatalytic activity of TiO_2 co-doping of graphene-Fe^{3+} ions for formaldehyde removal. *Journal of Environmental Management*, 127, 142-149.

[12] Adamu, H., Dubey, P. and Anderson, J.A., 2016. Probing the role of thermally reduced graphene oxide in enhancing performance of TiO_2 in photocatalytic phenol removal from aqueous environments. *Chemical Engineering Journal*, 284, 380-388.

[13] Yu, L., Wang, L., Sun, X. and Ye, D., 2018. Enhanced photocatalytic activity of rGO/TiO_2 for the decomposition of formaldehyde under visible light irradiation. *Journal of Environmental Science*, 73, 138-146.

[14] Sriwong, C., Choojun, K., Tejangkura, W. and Prasanseang, W., 2018. Preparation and photocatalytic activities of TiO_2-rGO nanocomposite catalysts for MB dye degradation over sunlight irradiation. *Materials Science Forum*, 936, 47-52.

[15] Chen, Y.-S., Chao, B.-K., Nagao, T. and Hsueh, C.-H., 2020. Effects of Ag particle geometry on photocatalytic performance of Ag/TiO_2/ reduced graphene oxide ternary systems. *Materials Chemistry and Physics*, 240, 122216, https://doi.org/10.1016/j.matchemphys.2019.122216.

[16] Salthammer, T., 2019. Formaldehyde sources, formaldehyde concentrations and air exchange rates in European housings. *Building and Environment*, 150, 219-232.

[17] WHO, 2010. *WHO Guidelines for Indoor Air Quality: Selected Pollutants*. Bohn: World Health Organization, European Centre for Environment and Health.

[18] ATSDR, 1999. *Toxicological Profile for Formaldehyde*. Georgia: Agency for Toxic Substances and Disease Registry.

[19] IARC, 2006. *IARC Monographs on the Evaluation of Carcinogenic Risks to Humans. Vol. 88: Formaldehyde, 2-butoxyethanol and 1-tert-butoxypropan-2-ol.* Lyon: International Agency for Research on Cancer.

[20] Ye, J.W., Zhu, X.F., Cheng, B., Yu, J.G. and Jiang, C.J., 2017. Few-layered graphene-like boron nitride: a highly efficient adsorbent for indoor formaldehyde removal. *Environmental Science and Technology Letters*, 4, 20-25.

[21] Zhu, X.B., Gao, X., Qin, R., Zeng, Y.X., Qu, R.Y., Zheng, C.H. and Tu, X., 2015. Plasma-catalytic removal of formaldehyde over Cu-Ce catalysts in a dielectric barrier discharge reactor. *Applied Catalysis B: Environmental*, 170, 293-300.

[22] Shao, Y., Wang, Y., Zhao, R., Chen, J., Zhang, F., Linhardt, R.J. and Zhong, W., 2020. Biotechnology progress for removal of indoor gaseous formaldehyde. *Applied Microbiology and Biotechnology*, 104, 3715-3727.

[23] Chen, D., Qu, Z., Sun, Y. and Wang, Y., 2014. Adsorption-desorption behavior of gaseous formaldehyde on different porous Al_2O_3 materials. *Colloids and Surfaces A*, 441, 433-440.

[24] Bisht, S., Nautiyal, B., Bhatt, U.M. and Joshi, P., 2014. Plasma applications for environmental protection. *International Journal of Engineering and Advanced Technology,* 3(5), 77-81.

[25] Hänel, A., Janczarek, M., Lieder, M. and Hupka, J., 2019. Photocatalytic decomposition of air pollutants using electrodeposited photocatalysts on stainless steel. *Polish Journal of Environmental Studies*, 28(3), 1157-1164.

[26] Shan, A.Y., Ghazi, T.I.M. and Rashid, S.A., 2010. Immobilisation of titanium dioxide onto supporting materials in heterogeneous photocatalysis: A review. *Applied Catalysis A: General*, 389, 1-8.

[27] Huang, Y., Ho, S.S.H., Lu, Y., Niu, R., Xu, L., Cao, J. and Lee, S., 2016. Removal of indoor volatile organic compounds via photocatalytic oxidation: A short review and prospect. *Molecules*, 21(1), 56, https://doi.org/10.3390/molecules21010056.

[28] Khalid, N.R., Ahmed, E., Hong, Z., Zhang, Y., Ullah, M. and Ahmad, M., 2013. Graphene modified ND/TiO_2 photocatalyst for methyl orange degradation under visible light irradiation. *Ceramics International*, 39, 3569-3575.

[29] Phrompet, C., Sriwong, C. and Ruttanapun, C., 2019. Mechanical, dielectric, thermal and antibacterial properties of reduced graphene oxide (rGO)-nanosized C3AH6 cement nanocomposites for smart cement-based materials. *Composites Part B*, 175, 107128, https://doi.org/10.1016/j.compositesb.2019.107128.

[30] Khalid, N.R., Ahmed, E., Ahmad, M., Niaz, N.A., Ramzan, M., Shakil, M., Iqbal, T. and Majid, A., 2016. Microwave-assisted synthesis of Ag–TiO_2/graphene composite for hydrogen production under visible light irradiation. *Ceramics International*, 42(16), 18257-18263.

[31] Li, Y.X., Jiang, Y., Peng, S.Q. and Jiang, F.Y., 2010. Nitrogen-doped TiO_2 modified with NH_4F for efficient photocatalytic degradation of formaldehyde under blue light-emitting diodes. *Journal of Hazardous Materials*, 182, 90-96.

[32] Singhal, R.K., Gangadhar, B., Basu, H., Manisha, V., Naidu, G.R.K. and Reddy, A.V.R., 2012. Remediation of malathion contaminated soil using zero valent iron nano-particles. *American Journal of Analytical Chemistry*, 3, 76-82.

[33] Castrejón-Sánchez, V.H. and Camacho-López, M., 2014. Quantification of phase content in TiO_2 thin films by Raman spectroscopy. *Superficies y Vacío*, 27(3), 88-92.

[34] Sukumaran, S.S., Rekha, C.R., Resmi, A.N., Jinesh, K.B. and Gopchandran, K.G., 2018. Raman and scanning tunneling spectroscopic investigations on graphene-silver nanocomposites. *Journal of Science: Advanced Materials and Devices*, 3(3), 353-358.

[35] Ali, T., Ahmed, A., Alam, U., Uddin, I., Tripathi, P. and Muneer, M., 2018. Enhanced photocatalytic and antibacterial activities of Ag-doped TiO_2 nanoparticles under visible light. *Materials Chemistry and Physics*, 212, 325-335.

[36] Hu, X., Li, C., Sun, Z., Song, J. and Zheng, S., 2020. Enhanced photocatalytic removal of indoor formaldehyde by ternary heterogeneous BiOCl/TiO_2/sepiolite composite under solar and visible light. *Building and Environment*, 168, 106481. https://doi.org/10.1016/j.buildenv. 2019.106481.

[37] Leong, K.H., Sim, L.C., Bahnemann, D., Jang, M., Ibrahim, S. and Saravanan, P., 2015. Reduced graphene oxide and Ag wrapped TiO_2 photocatalyst for enhanced visible light photocatalysis. *APL Materials*, 3, 104503, https://doi.org/10.1063/1.4926454.

[38] Umrao, S., Abraham, S., Theil, F., Pandey, S., Ciobota, V., Shukla, P.K., Rupp, C.J., Chakraborty, S., Ahuja, R. and Popp, J., 2014. A possible mechanism for the emergence of an additional band gap due to a Ti-O-C bond in the TiO_2-graphene hybrid system for enhanced photodegradation of methylene blue under visible light. *RSC Advances*, 4, 59890-59901.

[39] Yoon, H., Kim, D., Park, M., Kim, J., Kim, J., Srituravanich, W., Shin, B., Jung, Y. and Jeon, S., 2018. Extraordinary enhancement of UV absorption in TiO_2 nanoparticles enabled by low-oxidized grapheme nanodots. *Journal of Physical Chemistry C*, 122(22), 12114-12121.

[40] Ohko, Y., Hashimoto, K. and Fujishima, A., 1997. Kinetics of photocatalytic reactions under extremely low-intensity UV illumination on titanium dioxide thin films. *Journal of Physical Chemistry A*, 101, 8057-8062.

[41] Kirchnerova, J., Cohen, M.L.H., Guy, C. and Klvana, D., 2005. Photocatalytic oxidation of n-butanol under fluorescent visible light lamp over commercial TiO_2 (Hombicat UV100 and Degussa P25). *Applied Catalysis A: General*, 282, 321-332.

[42] Noguchi, T., Fujishima, A., Sawunyama, P. and Hashimoto, K., 1998. Photocatalytic degradation of gaseous formaldehyde using TiO_2 film. *Environmental Science and Technology*, 32(23), 3831-3833.